Research Article

Liproxstatin-1 is an effective inhibitor of oligodendrocyte ferroptosis induced by inhibition of glutathione peroxidase 4

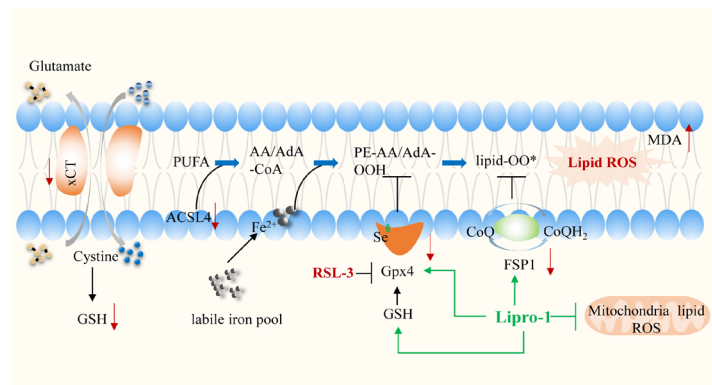Bao-You Fan[1, #], Yi-Lin Pang[1, #], Wen-Xiang Li[1, #], Chen-Xi Zhao[1], Yan Zhang[1], Xu Wang[1], Guang-Zhi Ning[1], Xiao-Hong Kong[2], Chang Liu[2], Xue Yao[1, *], Shi-Qing Feng[1, *]

Graphical Abstract *Ferroptosis in OLN93 oligodendrocytes*

Abstract

Our previous studies showed that ferroptosis plays an important role in the acute and subacute stages of spinal cord injury. High intracellular iron levels and low glutathione levels make oligodendrocytes vulnerable to cell death after central nervous system trauma. In this study, we established an oligodendrocyte (OLN-93 cell line) model of ferroptosis induced by RSL-3, an inhibitor of glutathione peroxidase 4 (GPX4). RSL-3 significantly increased intracellular concentrations of reactive oxygen species and malondialdehyde. RSL-3 also inhibited the main anti-ferroptosis pathway, i.e., SLC7A11/glutathione/glutathione peroxidase 4 (xCT/GSH/GPX4), and downregulated acyl-coenzyme A synthetase long chain family member 4. Furthermore, we evaluated the ability of several compounds to rescue oligodendrocytes from ferroptosis. Liproxstatin-1 was more potent than edaravone or deferoxamine. Liproxstatin-1 not only inhibited mitochondrial lipid peroxidation, but also restored the expression of GSH, GPX4 and ferroptosis suppressor protein 1. These findings suggest that GPX4 inhibition induces ferroptosis in oligodendrocytes, and that liproxstatin-1 is a potent inhibitor of ferroptosis. Therefore, liproxstatin-1 may be a promising drug for the treatment of central nervous system diseases.

Key Words: cell death; central nervous system; factor; ferroptosis; oligodendrocyte; oxidation; pathway; repair; spinal cord injury

Chinese Library Classification No. R453; R741; Q255

Introduction

After traumatic central nervous system (CNS) injury, significant oligodendrocyte loss occurs as a result of secondary injury (Lytle and Wrathall, 2007; Oyinbo, 2011; Scheller et al., 2017). Death of oligodendrocytes leads to demyelination, which accounts for poor functional recovery. Because of low levels of glutathione (GSH) and high levels of iron, oligodendrocytes are highly susceptible to oxidative damage (Thorburne and Juurlink, 1996; Juurlink et al., 1998). Low glutathione and high iron are also key inducers of ferroptosis, a recently-discovered form of regulated cell death (Dixon et al., 2012). However, ferroptosis in oligodendrocytes has not been well-studied.

Glutathione peroxidase 4 (GPX4) is a central regulator of ferroptosis (Yang et al., 2014). In the spinal cord, GPX4 is mainly expressed in neurons and oligodendrocytes, but not in astrocytes (Hu et al., 2019). Numerous studies have investigated the mechanisms of ferroptosis in neurons (Chen et al., 2015; Zhang et al., 2018, 2020; Kenny et al., 2019; Chu et al., 2020). GPX4 plays a pivotal role in neuronal ferroptosis. Knockout of GPX4 in neurons results in ferroptosis (Chen et al., 2015). After spinal cord injury, GPX4 is downregulated, and the ferroptosis inhibitor SRS 16-86 and deferoxamine (DFO) can prevent this reduction in GPX4 and improve the survival of neurons in the injured spinal cord (Yao et al., 2019; Zhang et

[1]International Cooperation Base of Spinal Cord Injury, Tianjin Key Laboratory of Spine and Spinal Cord, Department of Orthopedics, Tianjin Medical University General Hospital, Tianjin, China; [2]School of Medicine, Nankai University, Tianjin, China

*Correspondence to: Xue Yao, Ph.D, xueyao@tmu.edu.cn; Shi-Qing Feng, PhD, MD, sqfeng@tmu.edu.cn.

https://orcid.org/0000-0003-4904-7697 (Xue Yao); https://orcid.org/0000-0001-9437-7674 (Shi-Qing Feng)

#These authors contributed equally to this study.

How to cite this article: *Fan BY, Pang YL, Li WX, Zhao CX, Zhang Y, Wang X, Ning GZ, Kong XH, Liu C, Yao X, Feng SQ (2021) Liproxstatin-1 is an effective inhibitor of oligodendrocyte ferroptosis induced by inhibition of glutathione peroxidase 4. Neural Regen Res 16(3):561-566.*

al., 2019). GPX4 is localized to the nucleus in oligodendrocytes *in vivo*, in contrast to the neuronal cytoplasmic localization (Hu et al., 2019). However, whether GPX4 also plays a key role in oligodendrocyte survival has not been investigated.

RSL-3 was discovered before ferroptosis, and it increases lethality in the presence of oncogenic Ras. RSL-3 was demonstrated to induce ferroptosis (Yang and Stockwell, 2008). Further research demonstrated that RSL-3 binds to and inhibits GPX4 (Yang et al., 2014). GPX4 is decreased during ferroptosis in intracerebral hemorrhage and spinal cord injury animal models (Zhang et al., 2018, 2019; Yao et al., 2019). Therefore, in this study, we used RSL-3 to investigate ferroptotic cell death induced by GPX4 inhibition in oligodendrocytes.

OLN93 is a permanent oligodendroglial cell line derived from neonatal rat brain. OLN93 cells express typical markers of oligodendrocytes, such as myelin basic protein, myelin-associated glycoprotein and proteolipid protein (Richter-Landsberg and Heinrich, 1996). It is a valid cell model for investigating the proliferation and differentiation of oligodendrocytes (Richter-Landsberg and Heinrich, 1996; Robitzki et al., 2000; Vargas-Medrano et al., 2019). Liproxstatin-1 (Lipro-1) is an inhibitor of ferroptosis, and our previous study demonstrated that DFO can inhibit ferroptosis. Edaravone (EDA) was recently reported to inhibit ferroptosis of hepatoma cells *in vitro* (Friedmann Angeli et al., 2014; Homma et al., 2019; Yao et al., 2019). In this study, we further examined the ability of these compounds to inhibit ferroptosis in oligodendrocytes. We established a model of ferroptosis induced by inhibition of GPX4 in OLN93 oligodendrocytic cells, and we compared the effects of different ferroptosis inhibitors, with the aim of helping to advance the development of strategies for inhibiting oligodendrocyte ferroptosis.

Materials and Methods

Cell culture
ONL-93 oligodendrocytes (Cat# LSMCE1331; Wuhan Vector Science Co., Ltd., Wuhan, China) were cultured and expanded in Dulbecco's modified Eagle medium/nutrient mixture F-12 (Cat# 11330057; Gibco, Carlsbad, CA, USA), supplemented with 10% fetal bovine serum (Cat# 16000044; Gibco) and 1% penicillin-streptomycin (Cat# 15140122; Gibco) at 37°C and 5% CO_2. The culture medium was changed every 2 days. For the experiments, the plates were coated with poly-L-lysine (Cat# A3890401; Gibco) overnight, and the cells were cultured in medium (Dulbecco's modified Eagle medium/nutrient mixture F-12 + 2% fetal bovine serum + 1% penicillin-streptomycin) in 96-well (4×10^3/well), 24-well (4×10^4/well) or 6-well (3×10^5/well) plates.

Immunofluorescence staining
Cells were washed with phosphate-buffered saline (PBS) and fixed with 4% formaldehyde for 10 minutes at room temperature. After washing with PBS, the cells were covered with blocking medium (0.25% Triton X-100 and 5% goat serum in PBS) for 1 hour at room temperature. Then, the cells were incubated with the primary antibodies overnight at 4°C. After washing, the cells were incubated with secondary antibodies for 1 hour at room temperature. 4′,6-diamidino-2-phenylindole (Cat# C0065; Beijing Solarbio Science & Technology, Beijing, China) was used for nuclear staining. Images were captured on a fluorescence microscope (Cat# TH4-200; Olympus, Tokyo, Japan) and analyzed with Image Pro-Plus 6.0 (https://www.mediacy.com/). Primary antibodies included GPX4 (rabbit; 1:100; Cat# ab125006; Abcam, Cambridge, MA, USA), oligodendrocyte transcription factor 2 (Oligo2; goat; 1:200; Cat# F2418; R&D Systems, Minneapolis, MN, USA) and ferroptosis suppressor protein 1 (FSP1, also known as AIFM2; rabbit; 1:200; Cat# BS7655; Bioss, Woburn, MA, USA). Secondary antibodies were Alexa Fluor 488-conjugated goat anti-rabbit IgG (H+L) (1:500; Cat# ab150077; Abcam) and Cy3-labeled goat anti-mouse IgG (H+L) (1:500; Cat# A0521; Beyotime Biotechnology, Shanghai, China).

Cell viability assay
Cells seeded in 96-well plates were used for cell viability assay. To determine the RSL-3 concentration for 50% cytotoxicity, the cells were treated with PBS (0.1%), dimethyl sulfoxide (DMSO; 0.1%; Sigma-Aldrich, St. Louis, MO, USA), or RSL-3 (Cat# S8155; Selleck, Shanghai, China) at 100, 50, 25, 12.5, 6.25, 3.125, 1.5625 or 0.78 μM. Every group had five replicates. After 24 hours of RSL-3 treatment, the medium was replaced with fresh medium (Dulbecco's modified Eagle medium/nutrient mixture F-12 + 2% fetal bovine serum + 1% penicillin-streptomycin). 3-(4,5-Dimethylthiazolyl-2)-2,5-diphenyltetrazolium bromide (MTT; 10 μL, 5 mg/mL; Cat# M2128; Sigma-Aldrich) was added to each well. After 4 hours, the medium was removed, 150 μL DMSO was added, and the optical density was read at 490 nm with a spectrophotometer (Multiskan; Thermo Fisher Scientific, Waltham, MA, USA). For the determination of mean effective concentration (EC50) of Lipro-1 (Cat# S7699; Selleck), EDA (Cat# IE0020; Beijing Solarbio Science & Technology) and DFO (Cat# D9533; Sigma-Aldrich), the cell viability assay was also used.

Western blot assay
Western blot assay was used to assess the expression of ferroptosis-associated proteins (GPX4, SLC7A11 (xCT) and acyl-coenzyme A synthetase long chain family member 4 (ACSL4)) in OLN93 cells treated with RSL-3 to induce ferroptosis. We also examined the effects of Lipro-1. The cells were lysed with radioimmunoprecipitation assay buffer supplemented with phenylmethylsulfonyl fluoride (a protease inhibitor; Cat# ST505; Beyotime Biotechnology) for 30 minutes at 4°C. After centrifugation at 12,000 × *g* for 15 minutes, the supernatant was collected, and a bicinchoninic acid protein assay kit (Cat# P0012S; Beyotime Biotechnology) was used to measure protein concentration. Then, 20 μg of total protein was resolved by sodium dodecyl sulfate-polyacrylamide gel electrophoresis and transferred onto a polyvinylidene difluoride membrane (Cat# BSP0161; Beijing Solarbio Science & Technology). The membrane was blocked with 5% milk in Tris-buffered saline containing 0.1% Tween-20 for 1 hour, and then incubated with primary antibodies at 4°C overnight. After washing with Tris-buffered saline containing 0.1% Tween-20, the membrane was incubated for 1 hour at room temperature with the secondary antibodies. BeyoECL Star (Cat# P0018AM; Beyotime Biotechnology) was used for the detection of the bands. The primary antibodies were GPX4 (1:5000; rabbit; Cat# ab125006; Abcam), xCT (1:5000; rabbit; Cat# ab175186; Abcam), ACSL4 (1:10,000; rabbit; Cat# ab155282; Abcam) and glyceraldehyde 3-phosphate dehydrogenase (1:1000; rabbit; Cat# 2118; Cell Signaling Technology, Danvers, MA, USA). Secondary antibodies were horseradish peroxidase-linked anti-rabbit IgG (1:2000; Cat# 7074; Cell Signaling Technology) and horseradish peroxidase-linked anti-mouse IgG (1:2000; Cat# 7076; Cell Signaling Technology).

Reactive oxygen species detection
A reactive oxygen species (ROS) assay kit (Cat# S0033; Beyotime Biotechnology) was used on cells seeded in 24-well plates. After washing with culture medium (3×), the cells were incubated with 10 mM dichloro-dihydro-fluorescein diacetate and 10 mM Hoechst 33342 (Cat# 14533; Sigma-Aldrich) for 20 minutes at 37°C. The cells were washed three times with warm culture medium. Images were obtained on a fluorescence microscope (Cat# TH4-200; Olympus). ROS levels were calculated based on fluorescence intensity.

GSH detection
For GSH detection, cells were treated with PBS (0.1%), DMSO

(0.1%), RSL-3 (7.89 μM) or RSL-3 (7.89 μM) + Lipro-1 (1 μM) for 24 hours. For the RSL-3 + Lipro-1 group, RSL-3 and Lipro-1 were added at the same time. A micro reduced GSH assay kit (Cat# BC1175; Beijing Solarbio Science & Technology) was used to measure the levels of GSH. The cells were collected after digestion and centrifugation, washed with PBS twice, and then lysed with three rounds of freezing and thawing. After centrifugation at 8000 × g for 10 minutes, the supernatant was collected. The GSH detection was conducted according to the product manual. The content of GSH in the samples was calculated according to the standard curve.

Malondialdehyde detection
Cells in the PBS (0.1%), dimethyl sulfoxide (DMSO; 0.1%), RSL-3 (7.89 μM) and RSL-3 (7.89 μM) + Lipro-1 (1 μM) groups were used for malondialdehyde (MDA) detection by an MDA assay kit (Cat# BC0025; Beijing Solarbio Science & Technology). Cell pellets were collected by centrifugation, 1 mL extract solution was added, and cells were lysed by ultrasonication. After centrifugation at 8000 × g at 4°C for 10 minutes, the supernatants were collected and used to detect MDA levels. The optical densities were read at 450, 532 and 600 nm. The amount of MDA was obtained using the formula provided in the product manual.

Propidium iodide staining
Propidium iodide (PI) solution (20 μM in PBS; Cat# P8080; Beijing Solarbio Science & Technology) was used to detect dead cells. Cells in the wells were incubated with 500 μL culture medium supplemented with 50 μL PI solution and 5 μL Hoechst 33342 solution. Then, the cells were incubated at 37°C for 20 minutes. After washing with PBS, the cells were observed with a fluorescence microscope.

Mitochondrial lipid peroxidation detection
For mitochondrial lipid peroxidation detection, cells were divided into PBS (0.1%), DMSO (0.1%), RSL-3 (7.89 μM) and RSL-3 (7.89 μM) + Lipro-1 (1 μM) groups. 3-[4-(Perylenylphenylphosphino)phenoxy] propyltriphenylphosphonium iodide (MitoPeDPP; Cat# 466; Dojindo Molecular Technologies, Rockville, MD, USA) was used to detect mitochondrial lipid peroxidation. Culture medium was removed, and the cells were washed with PBS. MitoPeDPP working solution (100 μL) was added to each well and incubated at 37°C for 15 minutes in the dark. The supernatant was discarded, and the wells were washed with PBS. PBS with reagent was added, and the cells were observed under a fluorescence microscope.

Statistical analysis
The data are shown as the mean ± standard deviation (SD), and were analyzed using one-way analysis of variance followed by Tukey's *post hoc* test. Statistical significance was set at $P < 0.05$. The data were analyzed with GraphPad Prism 7 (GraphPad Software, San Diego, CA, USA).

Results

RSL-3 induces the ferroptosis of OLN93 oligodendrocytes
In the spinal cord, whereas GPX4 localization is mostly cytoplasmic in neurons, it is mainly nuclear in oligodendrocytes (Hu et al., 2019). Our *in vitro* experiment revealed similar nuclear localization of Oligo2 and GPX4 in OLN93 oligodendrocytes by immunostaining (**Figure 1A** & **B**), consistent with *in vivo* observations in the mouse spinal cord (Hu et al., 2019).

After spinal cord injury, GPX4 is downregulated (Yao et al., 2019; Zhang et al., 2019). To examine the effect of GPX4 inhibition on oligodendrocytes, OLN93 oligodendrocytes were incubated with the GPX4 inhibitor RSL-3 at a concentration range of 0–100 μM. The cell viability decreased in a dose-

dependent manner, and the concentration for 50% cytotoxicity was 7.89 μM for RSL-3 (**Figure 1C**). PI staining confirmed the RSL-3-induced cell death (**Figure 1D**). ROS were significantly increased in the RSL-3 group compared with DMSO group ($P < 0.01$; **Figure 1E** and **F**).

The ferroptosis pathway is involved in the death of oligodendrocytes
GPX4 is a central regulator of ferroptosis, and its inhibition leads to ferroptosis. After treatment with RSL-3, GPX4 expression was significantly decreased ($P < 0.01$; **Figure 2A** and **B**). xCT, another key ferroptosis inhibitor, was also decreased in the RSL-3 group compared with the DMSO group ($P < 0.05$; **Figure 2C** and **D**). The ferroptosis marker ACSL4 was reduced in the RSL-3 group compared with the DMSO group ($P < 0.01$; **Figure 2E** and **F**). Collectively, these results suggest that key ferroptotic proteins are involved in the cell death of oligodendrocytes.

The EC50 of Lipro-1 is lower than that of EDA or DFO in the ferroptosis model
The cytoprotective effects of Lipro-1, EDA and DFO were compared with the MTT cell viability assay. As shown in **Figure**
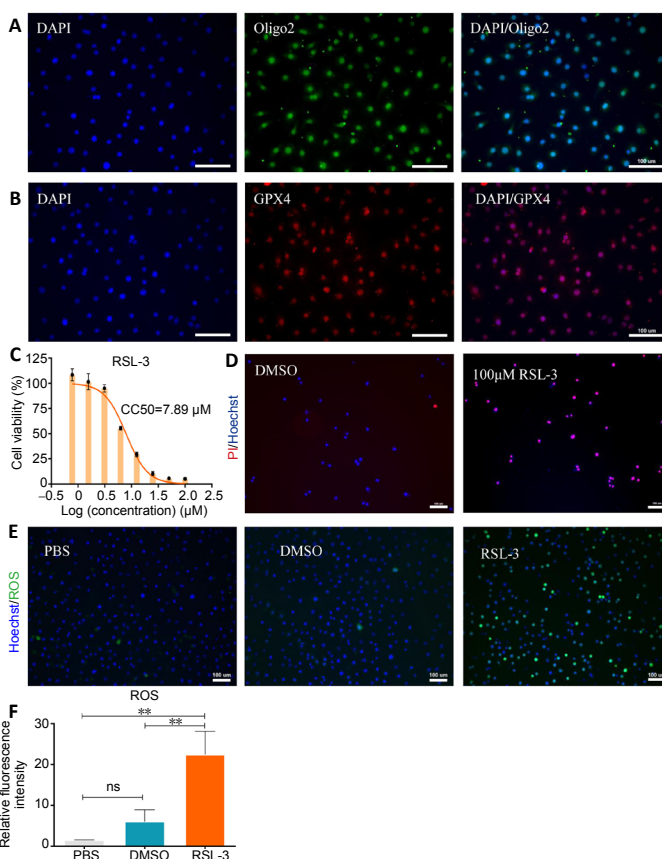
Figure 1 │ **RSL-3 induces the death of OLN93 oligodendrocytes.**
(A) OLN93 oligodendrocytes express Oligo2, which is mainly nuclear. The fluorescent indicator is Alexa Fluor 488 for Oligo2 (green). (B) GPX4 is mainly expressed in the nucleus of OLN93 oligodendrocytes. The fluorescent indicator is Cy3 for GPX4 (red). (C) After incubation with RSL-3 for 24 hours, the viability of OLN93 oligodendrocytes was decreased in a dose-dependent manner (CC50 of RSL-3 was 7.89 μM). The cell viability was assessed by MTT ($n = 5$). (D) Cell death was confirmed by PI and Hoechst 33342 staining for 24 hours ($n = 3$). The concentration of RSL-3 was 7.89 μM. (E, F) ROS accumulated following treatment with RSL-3 (7.89 μM) in OLN93 oligodendrocytes at 24 hours ($n = 3$). Scale bars: 100 μm. Data are expressed as the mean ± SD. **$P < 0.01$ (one-way analysis of variance followed by *post hoc* Tukey's test). CC50: Cytotoxicity concentration 50%; DAPI: 4′,6-diamidino-2-phenylindole; DMSO: dimethyl sulfoxide; GPX4: glutathione peroxidase 4; MTT: 3-(4,5-dimethylthiazol-2-yl)-2,5-diphenyltetrazolium bromide; Oligo2: oligodendrocyte transcription factor 2; PBS: phosphate-buffered saline; PI: propidium iodide; ROS: reactive oxygen species.

Research Article

3A, Lipro-1 suppressed ferroptosis, with an EC50 of 115.3 nM. EDA also suppressed ferroptosis, with an EC50 of 19.37 μM (**Figure 3B**). For DFO, the EC50 was 12.04 μM (**Figure 3C**). These results show that the EC50 of Lipro-1 was the lowest among these compounds (**Figure 3D**). Furthermore, the percentage of PI-positive cells was lower in the Lipro-1 group than in the RSL-3 group, providing further evidence of an anti-ferroptotic effect of Lipro-1 ($P < 0.0001$; **Figure 3E** and **F**).

Lipro-1 inhibits lipid peroxidation and restores the expression of GSH, GPX4 and FSP1

To further clarify the mechanisms by which Lipro-1 protects against ferroptosis in oligodendrocytes, lipid peroxidation was assessed. Compared with the PBS and DMSO groups, MDA levels were increased in the RSL-3 group ($P < 0.0001$), but decreased in the RSL-3 + Lipro-1 group ($P < 0.001$; **Figure 4A**). Furthermore, Lipro-1 suppressed mitochondrial lipid peroxidation (**Figure 4B**). We also measured components of the anti-ferroptotic GSH/GPX4 pathway. As shown in **Figure 4C**, Lipro-1 treatment increased the levels of GSH compared with the RSL-3 group ($P < 0.0001$). GPX4 was restored to normal levels by Lipro-1 treatment (**Figure 4D** and **E**). FSP1, a lipophilic radical-trapping antioxidant (Doll et al., 2019), was decreased by RSL-3. However, in the Lipro-1 group, the expression of FSP1 returned to normal (**Figure 4F**).

Discussion

We found here that GPX4 inhibition induces ferroptosis in oligodendrocytes, revealing the important role of the protein in oligodendrocyte survival. The key ferroptosis regulators xCT, GSH, GPX4 and ACSL4 were decreased during RSL-3-induced ferroptosis. Lipro-1 was more potent than EDA or DFO in rescuing oligodendrocytes from ferroptosis. Lipro-1 suppressed mitochondrial lipid peroxidation and reduced MDA levels, and it upregulated GSH, GPX4 and FSP1. Lipro-1 may therefore inhibit ferroptosis through these mechanisms.

We used OLN93 to investigate ferroptosis in oligodendrocytes. OLN93 is a cell line that expresses oligodendrocyte markers, such as myelin basic protein, myelin-associated glycoprotein, proteolipid protein and Oligo2, but not glial fibrillary acidic protein (Richter-Landsberg and Heinrich, 1996). Numerous studies have used this cell line to investigate various biological processes in oligodendrocytes, such as oxidative stress (Lim et al., 2016; Vargas-Medrano et al., 2019) and the inflammatory response (Askari and Shafiee-Nick, 2019).

We successfully induced ferroptosis in OLN93 cells with RSL-3. RSL-3 is a ferroptosis inducer that covalently binds and inhibits GPX4. After treatment with RSL-3, ROS and mitochondrial lipid peroxidation increased, which indicated that the function of GPX4 was suppressed. Our finding is consistent with other studies showing that GPX4 is downregulated by RSL-3 (Shin et al., 2018; Sui et al., 2018). xCT was also downregulated by RSL-3. xCT is a key regulator of ferroptosis (Jiang et al., 2015; Conrad et al., 2016). It is a light-chain subunit of system Xc⁻, which exchanges cystine in the extracellular space for glutamate. The cystine is then used to synthesis GSH. Thus, a downregulation of xCT would aggravate ferroptosis in oligodendrocytes. Erastin-induced ferroptotic cell death in primary cortical neurons is associated with decreased xCT and GPX4 (Zhang et al., 2020). Thus, the whole ferroptosis system (xCT and GPX4 mainly) is affected during ferroptosis. ACSL4 is a sensitive marker of ferroptosis (Doll et al., 2017). However, ACSL4 was downregulated in the present oligodendrocyte ferroptosis model. Because the dose of RSL-3 used here was based on the half-maximal inhibitory concentration (IC_{50}), the cells were not completely dead. Thus, cells might downregulate ACSL4 to modulate the lipid composition to suppress ferroptosis.

Oligodendrocytes are sensitive to oxidative stress, and are therefore more susceptible to ferroptosis. GSH is consumed by GPX4 to inhibit lipid peroxidation, especially of lipid hydroperoxides within biological membranes (Brigelius-Flohé and Maiorino, 2013). GPX4 protects against lipid peroxidation
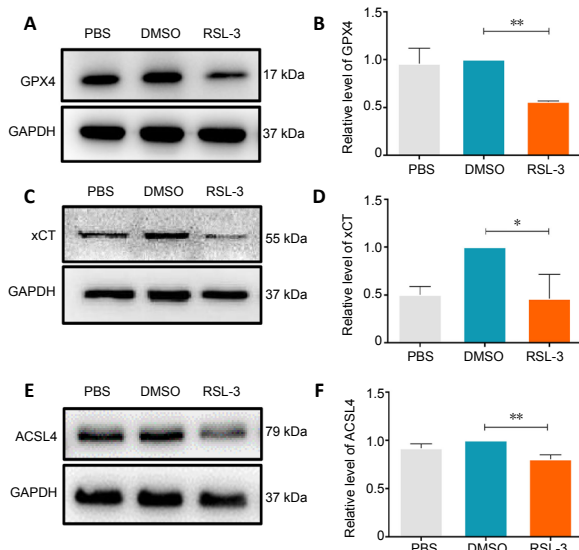

Figure 2 │ The expression of ferroptosis-associated pathway proteins in oligodendrocytes detected by western blot assay.
(A–F) The expression of GPX4 (A, B), xCT (C, D) and ACSL4 (E, F). The expression levels (standardized based on the GAPDH level first and then calculated relative to the DMSO group) of xCT, GPX4 and ACSL4 were decreased in the RSL-3 (7.89 μM) group compared with the DMSO group. Data are expressed as the mean ± SD ($n = 3$). *$P < 0.05$, **$P < 0.01$ (one-way analysis of variance followed by Tukey's *post hoc* test). ACSL4: Acyl-coenzyme A synthetase long chain family member 4; DMSO: dimethyl sulfoxide; GAPDH: glyceraldehyde 3-phosphate dehydrogenase; GPX4: glutathione peroxidase 4; PBS: phosphate-buffered saline; xCT: SLC7A11.
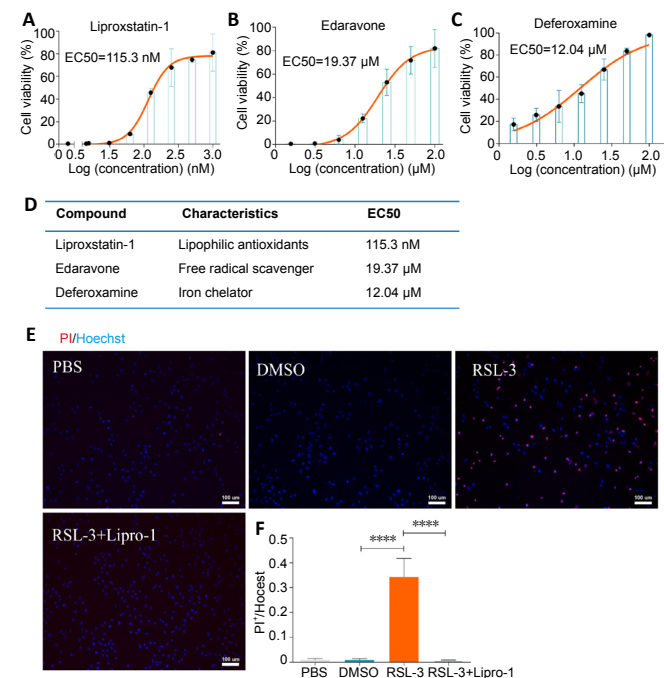
Figure 3 │ The inhibitory effects of Lipro-1, edaravone and deferoxamine on ferroptosis of OLN93 oligodendrocytes at 24 hours.
(A–C) The EC50 of Lipro-1 (A), edaravone (B) and deferoxamine (C) against ferroptosis in OLN93 oligodendrocytes ($n = 5$). (D) Characteristics and EC50 of Lipro-1, edaravone and deferoxamine. (E, F) Death of OLN93 oligodendrocytes treated with RSL-3 (7.89 μM) and Lipro-1 (1 μM) ($n = 3$). Scale bars: 100 μm. Data are expressed as the mean ± SD. ****$P < 0.0001$ (one-way analysis of variance followed by Tukey's *post hoc* test). DMSO: Dimethyl sulfoxide; EC50: mean effective concentration; Hoechst: Hoechst 33342; Lipro-1: liproxstatin-1; PBS: phosphate-buffered saline; PI: propidium iodide.
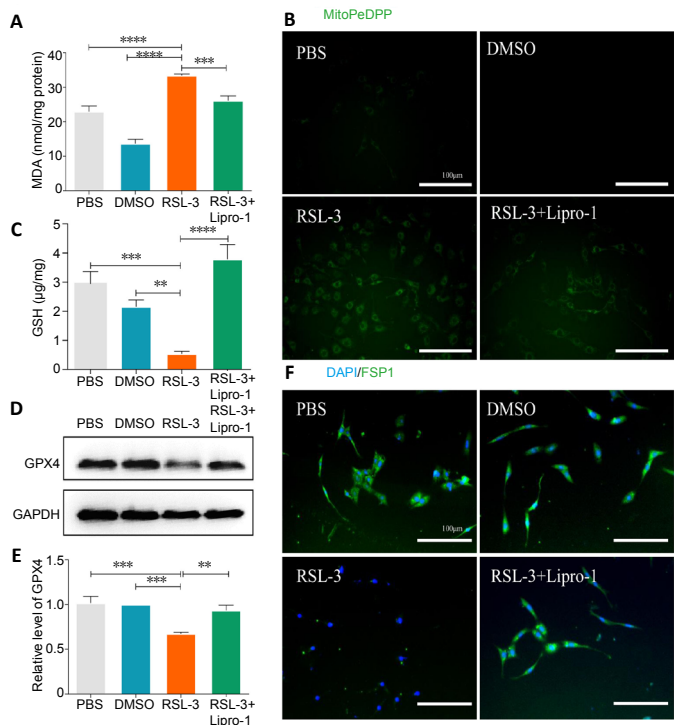
Figure 4 | Mechanism of Lipro-1-mediated inhibition of ferroptosis in OLN93 oligodendrocytes.
To observe the maximal effect of Lipro-1, the dose of Lipro-1 was 1 μM, and the dose of RSL-3 was 7.89 μM. (A) MDA levels. (B) Mitochondrial lipid peroxidation. Lipro-1 suppressed mitochondrial lipid peroxidation. (C) GSH levels. (D, E) Relative expression of GPX4. (F) Number of FSP1-positive cells. Lipro-1 restored FSP1-positive cells. The fluorescent indicator is Alexa Fluor 488 for FSP1 (green). Scale bars: 100 μm. Data are expressed as the mean ± SD ($n = 3$). **$P < 0.01$, ***$P < 0.001$, ****$P < 0.0001$ (one-way analysis of variance followed by Tukey's *post hoc* test). DAPI: 4′,6-Diamidino-2-phenylindole; DMSO: dimethyl sulfoxide; FSP1: ferroptosis suppressor protein 1; GAPDH: glyceraldehyde 3-phosphate dehydrogenase; GPX4: glutathione peroxidase 4; GSH: glutathione; Lipro-1: liproxstatin-1; MDA: malondialdehyde; MitoPeDPP: 3-[4-(perylenylphenylphosphino)phenoxy] propyltriphenylphosphonium iodide; PBS: phosphate-buffered saline.

by converting the reduced GSH into glutathione disulfide and the lipid hydroperoxides or hydrogen peroxide to the corresponding alcohol and/or water (Ursini et al., 1982; Brigelius-Flohé and Maiorino, 2013; Gaschler et al., 2018). However, the levels of GSH in oligodendrocytes are lower than those in astrocytes (Thorburne and Juurlink, 1996), and therefore the GSH/GPX4 system is insufficient to prevent lipid peroxidation. Additionally, the total iron content in oligodendrocyte precursor cells is much higher than that in astrocytes (Thorburne and Juurlink, 1996). Iron is essential for ferroptosis because of its ability to generate ROS via redox reactions (Ray et al., 2012). The increased levels of iron and the inability to inhibit lipid peroxidation are both key factors that render oligodendrocytes sensitive to ferroptosis. Interestingly, the expression of GPX4 is downregulated in spinal cord and brain injuries. Thus, oligodendrocytes are likely to undergo ferroptosis in these diseases, which would in turn aggravate demyelination.

The inhibition of ferroptosis in oligodendrocytes is a promising therapeutic strategy for diseases of the CNS. Several drugs have been used to inhibit ferroptosis in different animal models. Our previous study demonstrated the effectiveness of DFO, an iron chelating agent, in repairing spinal cord injury (Yao et al., 2019). However, that study only examined the protective effect of DFO in neurons. Additionally, an *in vitro* study showed that the free radical scavenger EDA can inhibit ferroptosis (Homma et al., 2019). Lipro-1 was reported to inhibit ferroptosis caused by GPX4 deficiency in the kidney (Friedmann Angeli et al., 2014). Thus, to find the most potent drugs to treat CNS diseases, the effectiveness of Lipro-1, EDA and DFO in suppressing ferroptosis was evaluated. Lipro-1 inhibited ferroptosis at nanomolar concentrations, and was more effective than EDA or DFO. However, *in vivo* experiments are needed to rigorously assess the potential of Lipro-1 for the treatment of CNS diseases.

Lipro-1 not only suppressed mitochondrial lipid peroxidation, but also enhanced the anti-ferroptosis pathway. A previous study demonstrated that Lipro-1 could decrease mitochondrial ROS (Feng et al., 2019), consistent with our current results. In particular, Lipro-1 increased GSH to enhance the anti-ferroptosis system. Furthermore, Lipro-1 restored GPX4 to normal levels in ferroptotic oligodendrocytes. Feng et al. (2019) reported that Lipro-1 could restore the expression of GPX4 *in vivo*. The GPX4 in nuclei can inhibit oxidative damage to the nucleus to rescue cells. Lipro-1 restores GPX4 levels in ONL93 cells to inhibit the ferroptosis signal in the nucleus (Imai et al., 2017). Currently, there is no evidence that GPX4 in the nucleus protects against mitochondrial lipid peroxidation. Recently, Bersuker et al. (2019) and Doll et al. (2019) found that another component of the cellular anti-ferroptosis system, FSP1, can reduce coenzyme Q10 using NAD(P)H, and that the reduced coenzyme Q could trap lipid peroxyl radicals, in turn suppressing lipid peroxidation. RSL-3 downregulated FSP1 in oligodendrocytes here, although the mechanism is still unclear.

There are limitations to this study of oligodendrocyte ferroptosis. First, we used the OLN93 cell line in this preliminary study. Further study may require primary oligodendrocytes or oligodendrocyte progenitor cells. Whether mature oligodendrocytes and oligodendrocyte progenitor cells have different susceptibilities to ferroptosis is an interesting question. The proliferation, differentiation and migration of oligodendrocyte progenitor cells should also be investigated in the pathology of ferroptosis. Moreover, whether ferroptosis occurs *in vivo* in mature oligodendrocytes or oligodendrocyte progenitor cells should be investigated in SCI mouse models. Iron metabolic changes should be also studied in oligodendrocyte ferroptosis because the metal plays a key role in oligodendrocyte maturation and function. After spinal cord injury, oligodendrocytes are severely decreased, and demyelination accounts for poor functional recovery (Grossman et al., 2001). Our previous study showed that the xCT/GSH/GPX4 signaling pathway is significantly impaired (Yao et al., 2019; Zhang et al., 2019). However, whether our *in vitro* findings can be extended to *in vivo* systems remains an open question. Deferoxamine, an iron chelator, can protect cells from ferroptosis, while liproxstatin-1 maybe works as a ferroptosis saver by inhibiting lipid peroxidation. However, the specific mechanisms behind these two drugs are not still well-known, so liproxstatin-1 combined with deferoxamine may provide a new insight into mechanism and it may also result in a therapeutically superior effect. And our following research will explore this interesting topic in the near future.

This study is the first investigation on oligodendrocyte ferroptosis induced by the GPX4-specific inhibitor RSL-3. RSL-3 reduced the expression of GPX4, xCT and ACSL4, and lowered GSH levels. We also discovered Lipro-1 was more potent than EDA or DFO in protecting against ferroptosis. Lipro-1 inhibited lipid peroxidation and increased the levels of GSH, GPX4 and FSP1. Our findings offer a novel strategy for treating CNS diseases associated with oligodendrocyte loss.

Research Article

Institutional review board statement: *OLN93 cells are a commercial product and are not directly implanted in humans or animals. So this study did not involve ethics issues.*

Copyright license agreement: *The Copyright License Agreement has been signed by all authors before publication.*

Plagiarism check: *Checked twice by iThenticate.*

Peer review: *Externally peer reviewed.*

Open access statement: *This is an open access journal, and articles are distributed under the terms of the Creative Commons Attribution-Non-Commercial-ShareAlike 4.0 License, which allows others to remix, tweak, and build upon the work non-commercially, as long as appropriate credit is given and the new creations are licensed under the identical terms.*

References

Askari VR, Shafiee-Nick R (2019) Promising neuroprotective effects of β-caryophyllene against LPS-induced oligodendrocyte toxicity: A mechanistic study. Biochem Pharmacol 159:154-171.

Bersuker K, Hendricks JM, Li Z, Magtanong L, Ford B, Tang PH, Roberts MA, Tong B, Maimone TJ, Zoncu R, Bassik MC, Nomura DK, Dixon SJ, Olzmann JA (2019) The CoQ oxidoreductase FSP1 acts parallel to GPX4 to inhibit ferroptosis. Nature 575:688-692.

Brigelius-Flohé R, Maiorino M (2013) Glutathione peroxidases. Biochim Biophys Acta 1830:3289-3303.

Chen L, Hambright WS, Na R, Ran Q (2015) Ablation of the ferroptosis inhibitor glutathione peroxidase 4 in neurons results in rapid motor neuron degeneration and paralysis. J Biol Chem 290:28097-28106.

Chu J, Liu CX, Song R, Li QL (2020) Ferrostatin-1 protects HT-22 cells from oxidative toxicity. Neural Regen Res 15:528-536.

Conrad M, Angeli JP, Vandenabeele P, Stockwell BR (2016) Regulated necrosis: disease relevance and therapeutic opportunities. Nat Rev Drug Discov 15:348-366.

Dixon SJ, Lemberg KM, Lamprecht MR, Skouta R, Zaitsev EM, Gleason CE, Patel DN, Bauer AJ, Cantley AM, Yang WS, Morrison B, 3rd, Stockwell BR (2012) Ferroptosis: an iron-dependent form of nonapoptotic cell death. Cell 149:1060-1072.

Doll S, Proneth B, Tyurina YY, Panzilius E, Kobayashi S, Ingold I, Irmler M, Beckers J, Aichler M, Walch A, Prokisch H, Trümbach D, Mao G, Qu F, Bayir H, Füllekrug J, Scheel CH, Wurst W, Schick JA, Kagan VE, et al. (2017) ACSL4 dictates ferroptosis sensitivity by shaping cellular lipid composition. Nat Chem Biol 13:91-98.

Doll S, Freitas FP, Shah R, Aldrovandi M, da Silva MC, Ingold I, Grocin AG, Xavier da Silva TN, Panzilius E, Scheel CH, Mourão A, Buday K, Sato M, Wanninger J, Vignane T, Mohana V, Rehberg M, Flatley A, Schepers A, Kurz A, et al. (2019) FSP1 is a glutathione-independent ferroptosis suppressor. Nature 575:693-698.

Feng Y, Madungwe NB, Imam Aliagan AD, Tombo N, Bopassa JC (2019) Liproxstatin-1 protects the mouse myocardium against ischemia/reperfusion injury by decreasing VDAC1 levels and restoring GPX4 levels. Biochem Biophys Res Commun 520:606-611.

Friedmann Angeli JP, Schneider M, Proneth B, Tyurina YY, Tyurin VA, Hammond VJ, Herbach N, Aichler M, Walch A, Eggenhofer E, Basavarajappa D, Rådmark O, Kobayashi S, Seibt T, Beck H, Neff F, Esposito I, Wanke R, Förster H, Yefremova O, et al. (2014) Inactivation of the ferroptosis regulator Gpx4 triggers acute renal failure in mice. Nat Cell Biol 16:1180-1191.

Gaschler MM, Andia AA, Liu H, Csuka JM, Hurlocker B, Vaiana CA, Heindel DW, Zuckerman DS, Bos PH, Reznik E, Ye LF, Tyurina YY, Lin AJ, Shchepinov MS, Chan AY, Peguero-Pereira E, Fomich MA, Daniels JD, Bekish AV, Shmanai VV, et al. (2018) FINO(2) initiates ferroptosis through GPX4 inactivation and iron oxidation. Nat Chem Biol 14:507-515.

Grossman SD, Rosenberg LJ, Wrathall JR (2001) Temporal-spatial pattern of acute neuronal and glial loss after spinal cord contusion. Exp Neurol 168:273-282.

Homma T, Kobayashi S, Sato H, Fujii J (2019) Edaravone, a free radical scavenger, protects against ferroptotic cell death in vitro. Exp Cell Res 384:111592.

Hu CL, Nydes M, Shanley KL, Morales Pantoja IE, Howard TA, Bizzozero OA (2019) Reduced expression of the ferroptosis inhibitor glutathione peroxidase-4 in multiple sclerosis and experimental autoimmune encephalomyelitis. J Neurochem 148:426-439.

Imai H, Matsuoka M, Kumagai T, Sakamoto T, Koumura T (2017) Lipid peroxidation-dependent cell death regulated by GPx4 and ferroptosis. Curr Top Microbiol Immunol 403:143-170.

Jiang L, Kon N, Li T, Wang SJ, Su T, Hibshoosh H, Baer R, Gu W (2015) Ferroptosis as a p53-mediated activity during tumour suppression. Nature 520:57-62.

Juurlink BH, Thorburne SK, Hertz L (1998) Peroxide-scavenging deficit underlies oligodendrocyte susceptibility to oxidative stress. Glia 22:371-378.

Kenny EM, Fidan E, Yang Q, Anthonymuthu TS, New LA, Meyer EA, Wang H, Kochanek PM, Dixon CE, Kagan VE, Bayir H (2019) Ferroptosis contributes to neuronal death and functional outcome after traumatic brain injury. Crit Care Med 47:410-418.

Lim JL, van der Pol SM, Baron W, McCord JM, de Vries HE, van Horssen J (2016) Protandim protects oligodendrocytes against an oxidative insult. Antioxidants (Basel) 5:30.

Lytle JM, Wrathall JR (2007) Glial cell loss, proliferation and replacement in the contused murine spinal cord. Eur J Neurosci 25:1711-1724.

Oyinbo CA (2011) Secondary injury mechanisms in traumatic spinal cord injury: a nugget of this multiply cascade. Acta Neurobiol Exp (Wars) 71:281-299.

Ray PD, Huang BW, Tsuji Y (2012) Reactive oxygen species (ROS) homeostasis and redox regulation in cellular signaling. Cell Signal 24:981-990.

Richter-Landsberg C, Heinrich M (1996) OLN-93: a new permanent oligodendroglia cell line derived from primary rat brain glial cultures. J Neurosci Res 45:161-173.

Robitzki A, Döll F, Richter-Landsberg C, Layer PG (2000) Regulation of the rat oligodendroglia cell line OLN-93 by antisense transfection of butyrylcholinesterase. Glia 31:195-205.

Scheller A, Bai X, Kirchhoff F (2017) The role of the oligodendrocyte lineage in acute brain trauma. Neurochem Res 42:2479-2489.

Shin D, Kim EH, Lee J, Roh JL (2018) Nrf2 inhibition reverses resistance to GPX4 inhibitor-induced ferroptosis in head and neck cancer. Free Radic Biol Med 129:454-462.

Sui X, Zhang R, Liu S, Duan T, Zhai L, Zhang M, Han X, Xiang Y, Huang X, Lin H, Xie T (2018) RSL3 drives ferroptosis through GPX4 inactivation and ROS production in colorectal cancer. Front Pharmacol 9:1371.

Thorburne SK, Juurlink BH (1996) Low glutathione and high iron govern the susceptibility of oligodendroglial precursors to oxidative stress. J Neurochem 67:1014-1022.

Ursini F, Maiorino M, Valente M, Ferri L, Gregolin C (1982) Purification from pig liver of a protein which protects liposomes and biomembranes from peroxidative degradation and exhibits glutathione peroxidase activity on phosphatidylcholine hydroperoxides. Biochim Biophys Acta 710:197-211.

Vargas-Medrano J, Segura-Ulate I, Yang B, Chinnasamy R, Arterburn JB, Perez RG (2019) FTY720-Mitoxy reduces toxicity associated with MSA-like α-synuclein and oxidative stress by increasing trophic factor expression and myelin protein in OLN-93 oligodendroglia cell cultures. Neuropharmacology 158:107701.

Yang WS, Stockwell BR (2008) Synthetic lethal screening identifies compounds activating iron-dependent, nonapoptotic cell death in oncogenic-RAS-harboring cancer cells. Chem Biol 15:234-245.

Yang WS, SriRamaratnam R, Welsch ME, Shimada K, Skouta R, Viswanathan VS, Cheah JH, Clemons PA, Shamji AF, Clish CB, Brown LM, Girotti AW, Cornish VW, Schreiber SL, Stockwell BR (2014) Regulation of ferroptotic cancer cell death by GPX4. Cell 156:317-331.

Yao X, Zhang Y, Hao J, Duan HQ, Zhao CX, Sun C, Li B, Fan BY, Wang X, Li WX, Fu XH, Hu Y, Liu C, Kong XH, Feng SQ (2019) Deferoxamine promotes recovery of traumatic spinal cord injury by inhibiting ferroptosis. Neural Regen Res 14:532-541.

Zhang Y, Fan BY, Pang YL, Shen WY, Wang X, Zhao CX, Li WX, Liu C, Kong XH, Ning GZ, Feng SQ, Yao X (2020) Neuroprotective effect of deferoxamine on erastininduced ferroptosis in primary cortical neurons. Neural Regen Res 15:1539-1545.

Zhang Y, Sun C, Zhao C, Hao J, Zhang Y, Fan B, Li B, Duan H, Liu C, Kong X, Wu P, Yao X, Feng S (2019) Ferroptosis inhibitor SRS 16-86 attenuates ferroptosis and promotes functional recovery in contusion spinal cord injury. Brain Res 1706:48-57.

Zhang Z, Wu Y, Yuan S, Zhang P, Zhang J, Li H, Li X, Shen H, Wang Z, Chen G (2018) Glutathione peroxidase 4 participates in secondary brain injury through mediating ferroptosis in a rat model of intracerebral hemorrhage. Brain Res 1701:112-125.

C-Editor: Zhao M; S-Editors: Yu J, Li CH; L-Editors: Patel B, Yu J, Song CP; T-Editor: Jia Y